# Influence of C, Mn and Ni Contents on Microstructure and Properties of Strong Steel Weld Metals — Part II. Impact Toughness Gain from Manganese Reductions

E. Keehan*, L. Karlsson**, H.-O. Andrén* and H. K. D. H. Bhadeshia***

* Department of Experimental Physics, Chalmers University of Technology, SE – 412 96 Gothenburg, Sweden

** ESAB AB, P.O. Box 8004, SE – 402 77 Gothenburg, Sweden.

***University of Cambridge, Department of Materials Science and Metallurgy, Pembroke Street, Cambridge CB2 3QZ, U.K.

## Abstract

Two experimental high strength steel weld metals were produced with 7 wt. % nickel and manganese at 2 or 0.5 wt. %. Neural network predictions that Mn reductions increase toughness were confirmed with impact energy increasing from 32 to 113 J at –40 °C. High resolution microstructural investigations showed that both weld metals contained mainly martensite at interdendritic regions and predominantly bainite at dendrite core regions as a consequence of manganese and nickel segregation. In the high manganese weld metal significant amounts of coarse grained coalesced bainite formed whereas mainly upper bainite was seen with 0.5 wt. % manganese weld metal. Reducing manganese increased the transformation temperature promoting formation of upper bainite with a fine grain size and dramatically reduced the amount and size of coalesced bainite. Increased toughness was attributed to the finer grain size of bainite constituents and a more effectively tempered microstructure.

## Background

High strength steel is increasingly employed in greater amounts due to the many advantages it offers such as size and weight reduction in many applications. However the joining of high strength steel must take place in a controlled manner with particular attention placed on welding if both strength and toughness requirements are to be met [1–3]. Since the 1960's, many have carried out research by varying elemental composition and welding parameters with the hope
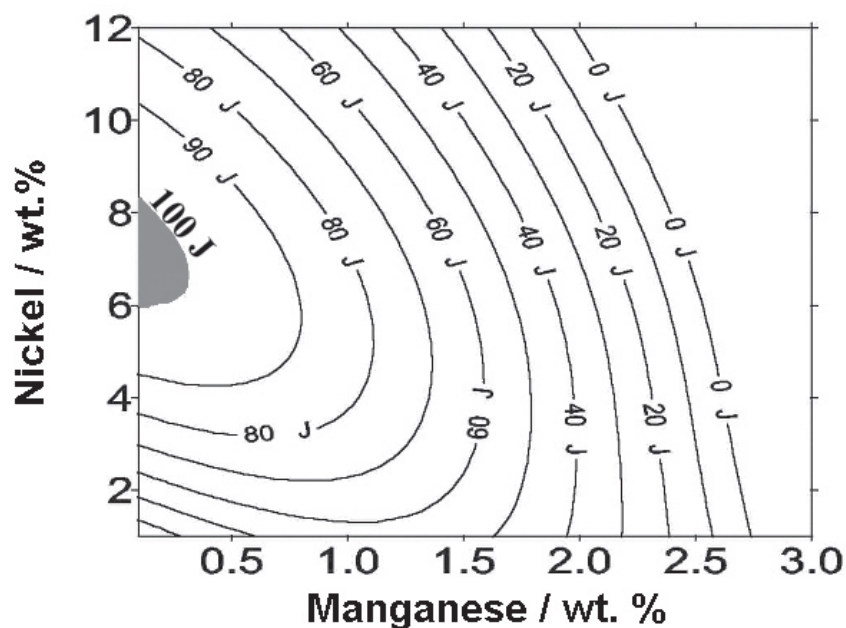
of achieving good strength above the region of 690 MPa (100 ksi) and toughness using shielded metal arc welding (SMAW).

The most promising results to date were achieved through the variation of Mn and Ni [4–6]. Zhang investigated a number of compositions with Mn less than 1.6 wt. % and Ni less than 5.5 wt %. With a combination of 0.36 Mn and 5.58 Ni, an toughness of ~55 J at –60 °C was recorded and a tensile strength of 904 MPa was predicted from hardness measurements. Increasing Mn to 0.7 wt % and reducing Ni to 3.5 wt % was found to increase impact toughness to ~75 J at –60 °C and a reduction in tensile strength to 745 MPa was predicted from hardness measurements. Mainly acicular ferrite with some Widmanstätten sideplates and grain boundary ferrite were reported while increasing nickel was found to promote martensite [4]. Lord investigated a similar composition and increased impact toughness to 74 J at –60 °C with Ni additions from 3 to 4 wt. % at decreasing Mn levels from 1.1 to 0.8 wt. %. Yield strength of 809 MPa was reported for this weld metal [5]. Recently an intermediate Mn content of 0.52 wt. % combined with 6.95 wt. % Ni was investigated. An impact toughness of 55 J at –60 °C was recorded and yield strength of 684 MPa was predicted with this composition. Microstructural investigations with light optical microscopy (LOM), reported various forms of ferrite and lath martensite [6].

These recorded mechanical properties were found to be in close agreement with neural network estimates where a contour plot suggested that the nickel and manganese concentrations must be optimised as shown in Figure 1 [7]. Based primarily on the neural network predictions, but also on literature, experimental weld metals were produced to study the changes in mechanical and microstructural behaviour in detail for Mn concentrations of 0.5 or 2.0 wt. % and Ni levels at 7 %. The present work is the second in a series of three papers that deal with the effects of changing nickel, manganese and carbon content in high strength steel weld metals. Microstructural characterisation is carried out with high resolution techniques such as field emission gun scanning electron microscopy (FEGSEM), transmission electron microscopy (TEM) and atom probe field ion microscopy (APFIM). Correlations are made between the microstructure and the mechanical properties.

**Experimental Procedures**

The welded joints were made as described previously [8]. The welding parameters and chemical compositions are presented in Table 1. The weld metals were named 7-2L250 and 7-0.5L250 where 7 is the nickel content, 2 or 0.5 is the manganese content, L stands for a low (0.03) carbon content and 250 is the interpass temperature in °C. Specimens for Charpy−V impact testing, tensile testing, dilatometry and metallographic analysis (LOM, FEGSEM and TEM) were prepared as previously described [8]. Secondary ion mass spectroscopy (SIMS) was also carried out on polished specimens in addition to energy dispersive X-ray analysis (EDX).
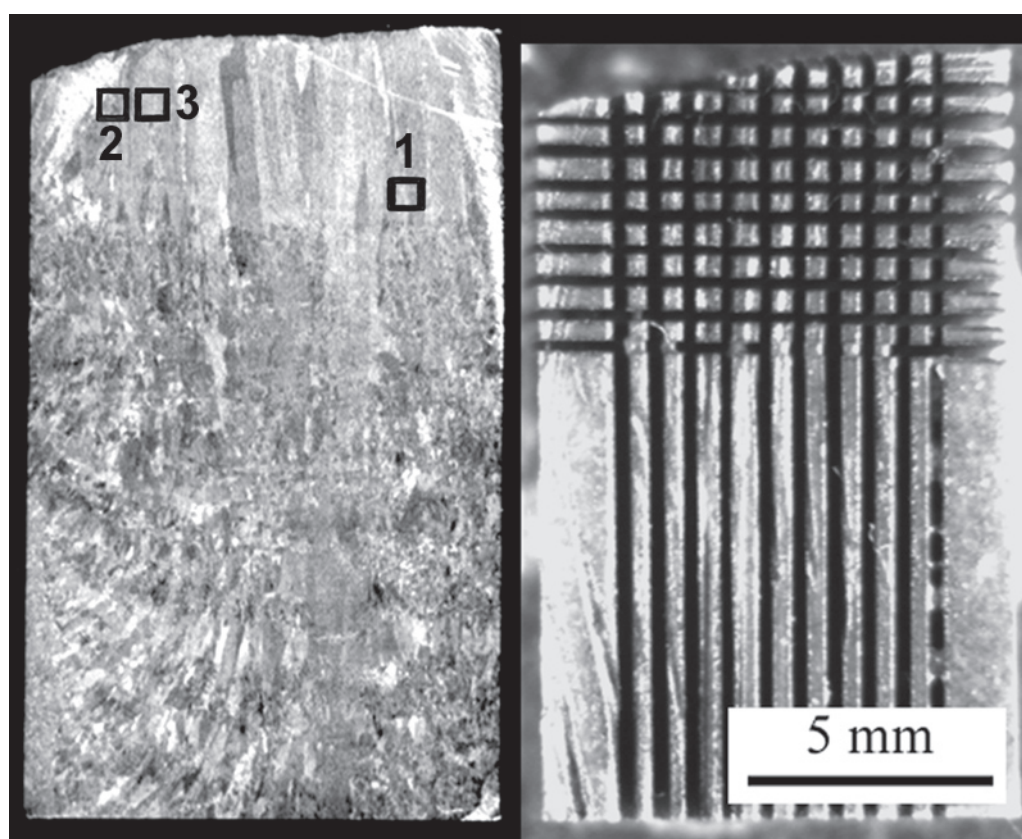
**Figure 1** Contour plot of impact toughness predictions at –40°C as a function of Ni and Mn content for the base composition of 0.034 C, 0.25 Si, 0.5 Cr and 0.62 Mo [7].

|  | 7-2L250 | 7-0.5L250 |
|---|---|---|
| E / kJ mm$^{-1}$ | 1.2 | 1 |
| IPT / °C | 250 | 250 |
| t$_{8/5}$ / s | 12 | 10 |
|  |  |  |
| C * | 0.032 | 0.024 |
| Mn | 2.02 | 0.64 |
| Ni | 7.23 | 6.6 |
| Cr | 0.47 | 0.21 |
| Si | 0.25 | 0.35 |
| S* | 0.008 | 0.008 |
| P | 0.011 | 0.012 |
| Mo | 0.63 | 0.4 |
| Cu | 0.03 | 0.03 |
| O / ppm* | 380 | 400 |
| N / ppm* | 250 | 197 |
|  |  |  |
| YS / MPa | 795 | 721 |
| UTS / MPa | 1006 | 823.5 |
| YS / UTS | 0.79 | 0.88 |
| A$_5$ / % | 15 | 21.3 |

**Table 1** Welding parameters, chemical composition and tensile properties. Welding parameters presented are energy input (E), interpass temperature (IPT) and the estimated cooling time between 800 and 500 °C (t$_{8/5}$) calculated from WeldCalc. [8] Composition is in wt. % unless otherwise stated and '*' indicate elements analysed using Leco Combustion equipment.

Atom probe field ion microscopy (APFIM) was performed on the last bead of both weld alloys in order to measure the carbon content of the ferritic matrix. Atom probe specimens were prepared by first removing a block of weld metal that included the last bead with approximate dimensions of $10 \times 10 \times 15$ mm. The bead structure of the weld metal was exposed using ammonium-peroxodisulphat and photographed. The block was then subjected to electric discharge machining (EDM) using a Charmilles Isopulse Type P25 discharge machine. Cuts were made parallel to the welding direction in order to produce rods with approximate dimensions, $0.4 \times 0.4 \times 10$ mm. On completion of EDM, the sample was again photographed to allow the rod locations to be traced as shown in Figure 2. Rods were then individually removed and electropolished to produce needle shape specimens with a tip radius of less that 50 nm using standard electropolishing methods [10]. All specimens were first examined using TEM to observe the shape of the needle, and in some cases the specimen was further electropolished to enhance the specimen shape. This final electropolishing was carried out applying short voltage pulses (10 V for 0.2 to 10 ms) which allows a controllable amount of material to be removed. Once satisfied with the specimen, it was investigated at specimen temperatures between 55 and 75 K. The residual gas pressure within the UHV chamber was kept below $7 \times 10^{-8}$ Pa and an evaporation pulse amplitude of 20 % of the standing voltage was applied. A description of the APFIM instrument and evaluation system may be found elsewhere [11–13].



**Figure 2** Image showing a block of weld metal from 7-2L250 before and after it was subjected to EDM machining. From this image it was possible to locate where the rods and in turn APFIM specimens were located in relation to the individual beads.

## Results

### Mechanical properties

The recorded tensile properties and Charpy–V impact toughness levels of these weld metals are presented in Table 1 and Figure 3. In short, it was confirmed that reducing manganese content from 2 to 0.5 wt % at 7 wt. % nickel leads to a large increase in toughness. As a result of this minor change in composition impact toughness increased from 32 J to 113 J at –40 °C. With this large increase of toughness, yield strength remained good with only a moderate decrease from 795 to 721 MPa.

### Microstructure – last bead

LOM micrographs from the last bead of the two weld metals are presented in Figure 4. Thermo-dynamic calculations presented elsewhere showed that both weld metals solidify as austenite [14] and the resulting dendritic segregation pattern is clearly seen in Figure 4. However without knowledge from high resolution methods it is difficult to say with certainty what microstructural constituents are present.

A representative FEGSEM micrograph from the last bead of weld metal 7-2L250 is shown in Figure 5. This micrograph is compatible with the LOM micrograph in Figure 4. With FEGSEM it was found that the microstructure was a mixture of upper and lower bainite along with a large grained bainitic constituent within the former dendrites while a lath-like microstructure
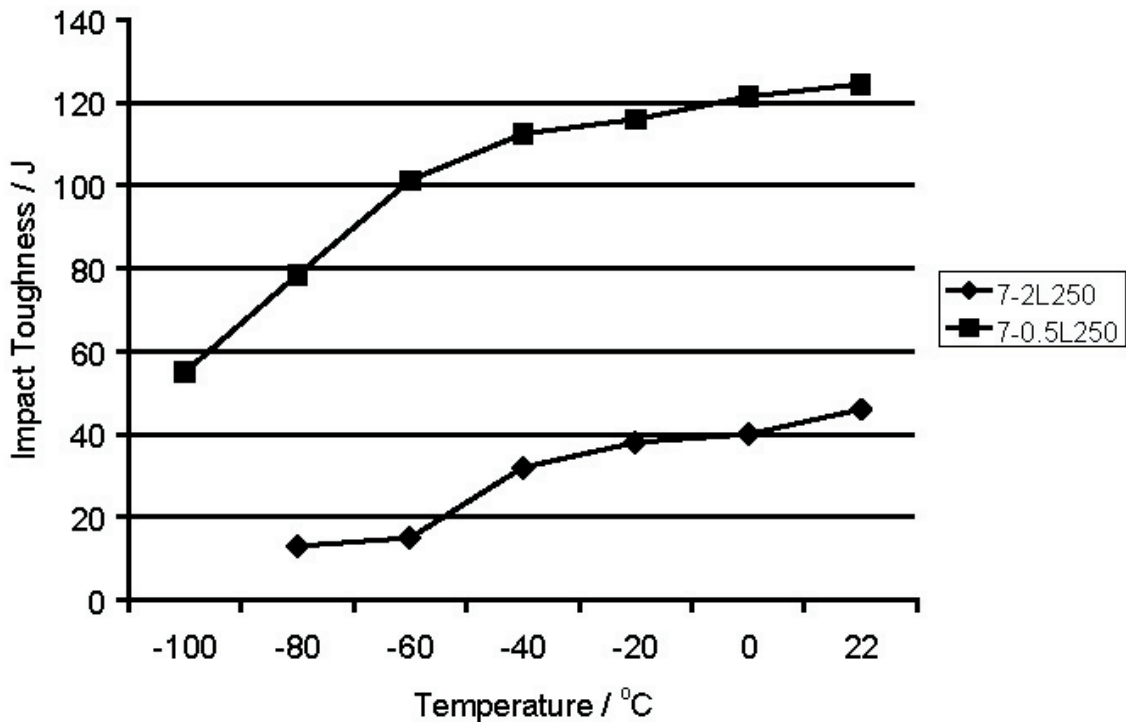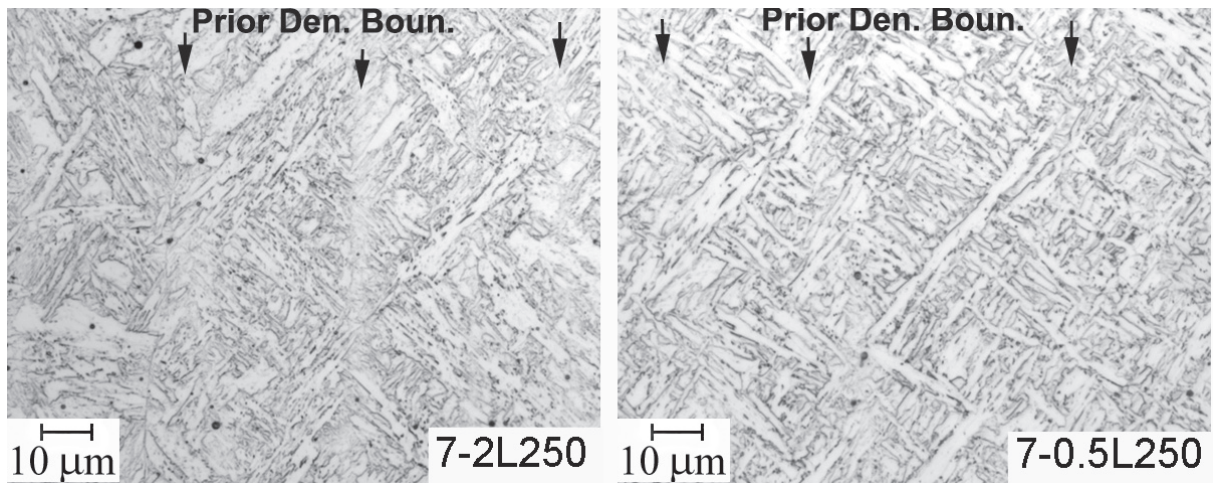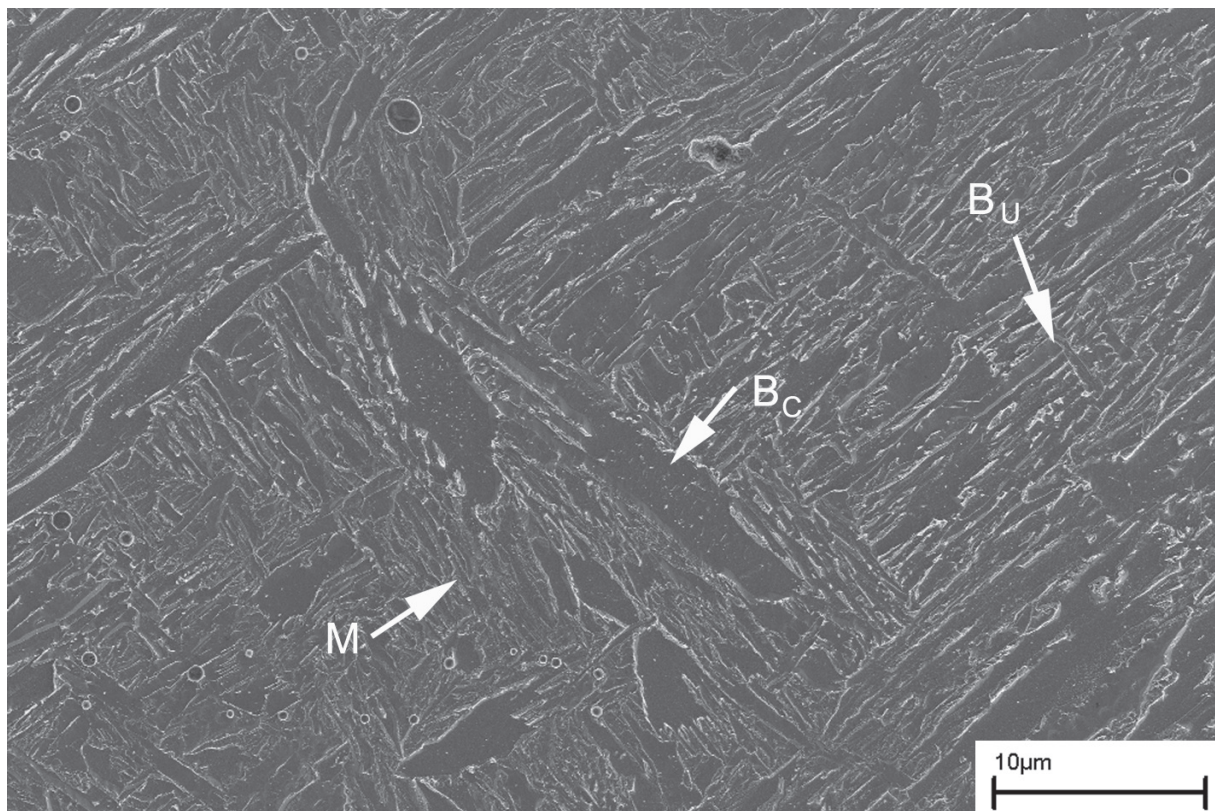


**Figure 3** The mean Charpy impact toughness recorded at each temperature.

**Figure 4** LOM micrograph of as-deposited weld metal. Here the effects of segregation during the dendritic solidification are clearly seen.
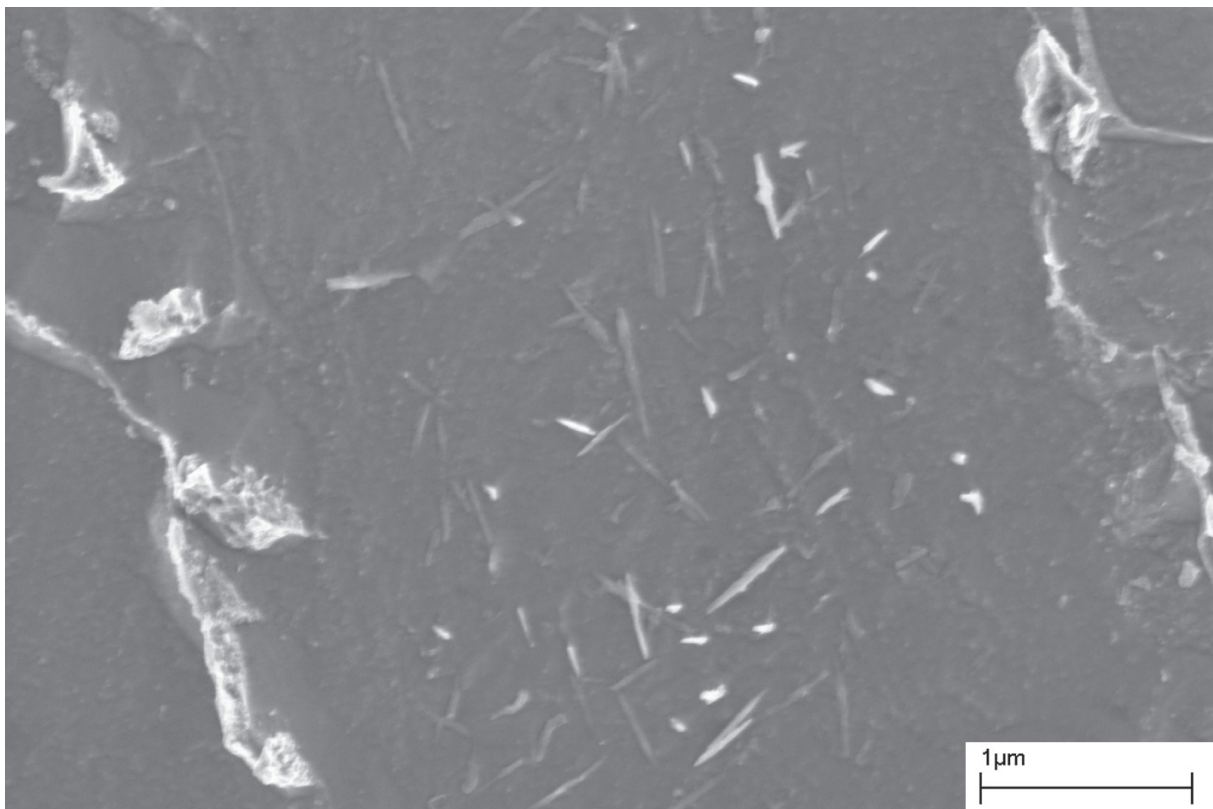


**Figure 5** An overview with FEGSEM of the microstructure in the last bead of 7-2L250. M is martensite, $B_U$ is upper bainite and $B_c$ is coalesced bainite.

of martensite was predominant at the prior dendrite boundaries. Figure 6 shows platelets of cementite precipitates within the large bainitic grains. Previously, extensive examinations of this constituent were carried out with high resolution techniques such as FEGSEM and TEM. It was found that very large bainitic ferrite grains formed without the typical subunit structure of platelets with cementite at boundaries. It was concluded that this constituent was that of coalesced bainite. Detailed results and discussion may be found elsewhere [15].
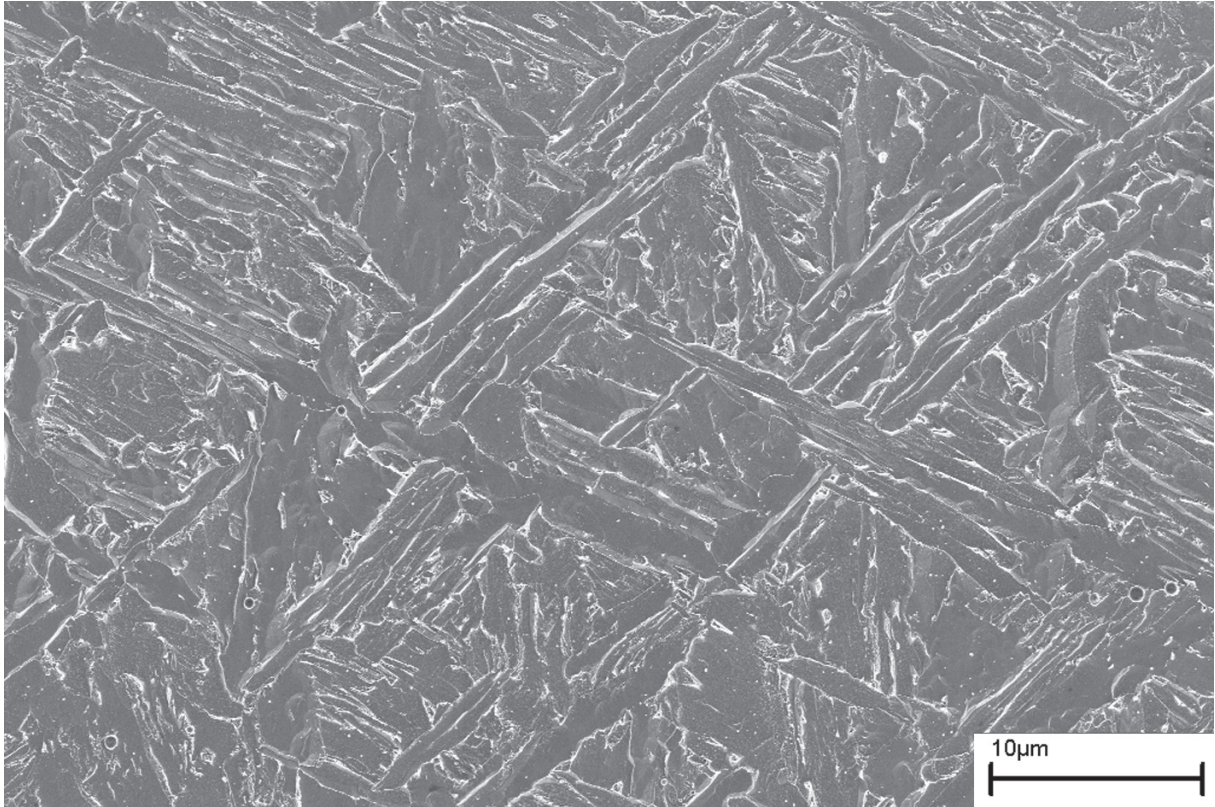
The microstructure of the last bead in the low manganese weld metal was also investigated with FEGSEM (Figure 7). It was found that the microstructure was mainly that of upper bainite with some lower bainite. Figure 8 shows a region of relatively coarse bainitic ferrite with some precipitates inside. The precipitates are spherical in nature rather than the plates seen in Figure 6. In both Figures 8 and 9 films are observed at boundaries while some martensite is also seen in Figure 9.

Selected micrographs from TEM investigations on the last bead of 7-2L250 are presented in Figures 10 and 11. A bright field image is shown together with a corresponding selected area diffraction pattern in Figure 10. The lattice parameters for the individual phases in steel are well known and corresponding distances for allowed reflections are well documented for given camera lengths [16–18]. In the diffraction pattern reflections were found that correspond to both ferrite and cementite. When a cementite spot was chosen to form a dark field image the black film in the bright field image was illuminated. Reducing the magnification in the dark field
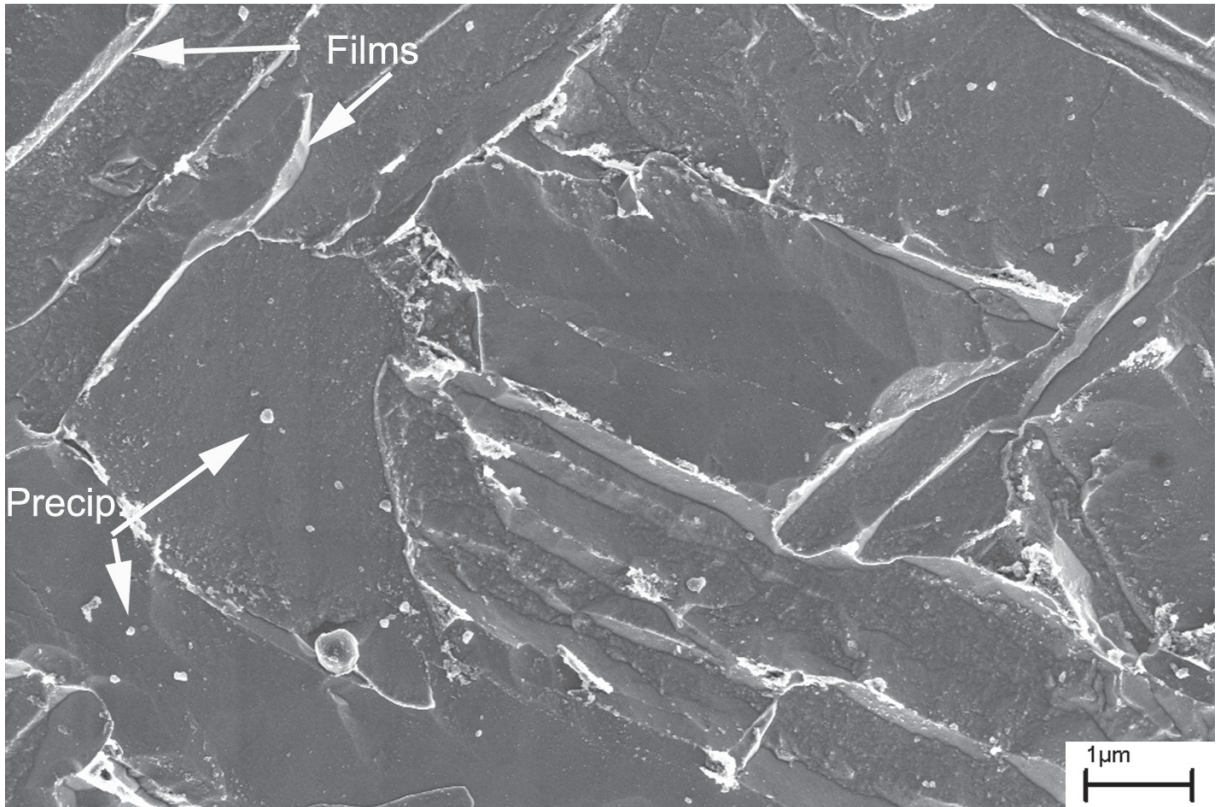


**Figure 6** Cementite platelets that form within coalesced bainite in as-deposited 2 Mn weld metal shown using FEGSEM.
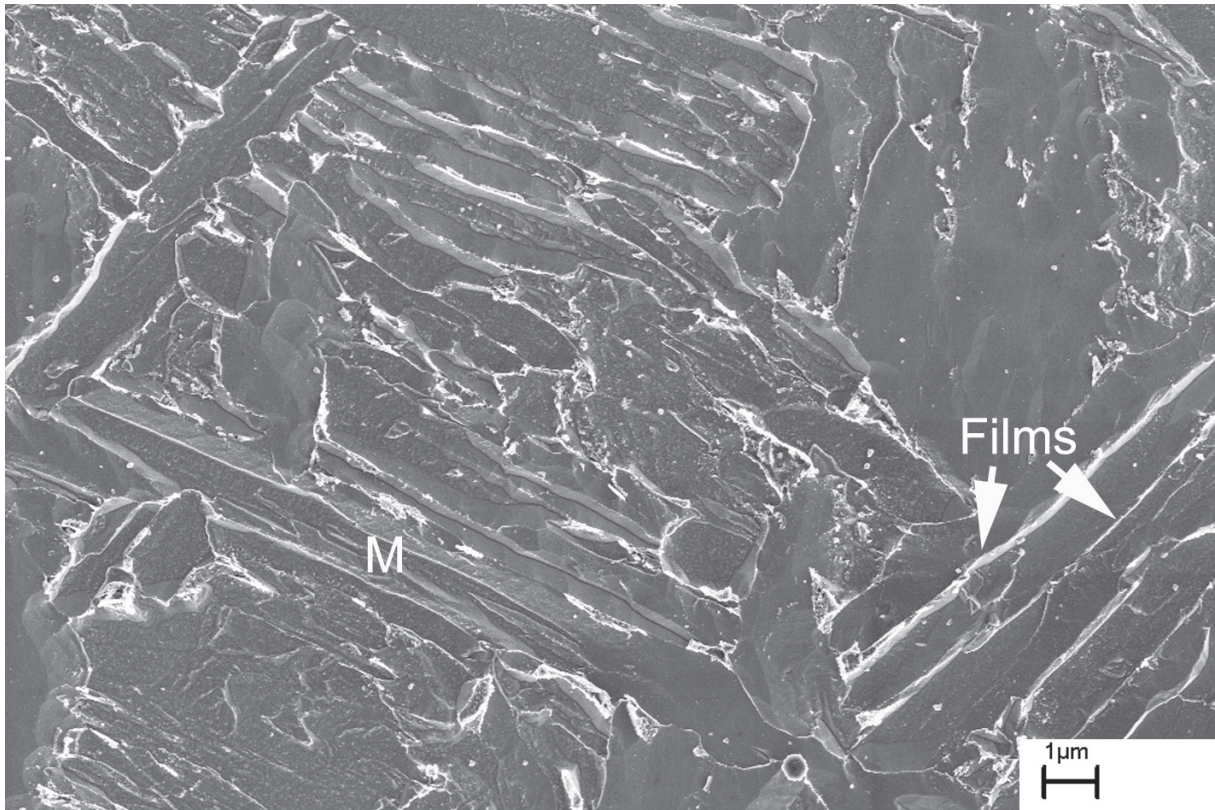
**Figure 7** An overview of the microstructure in the last bead formed with 0.5 Mn using FEG-SEM.
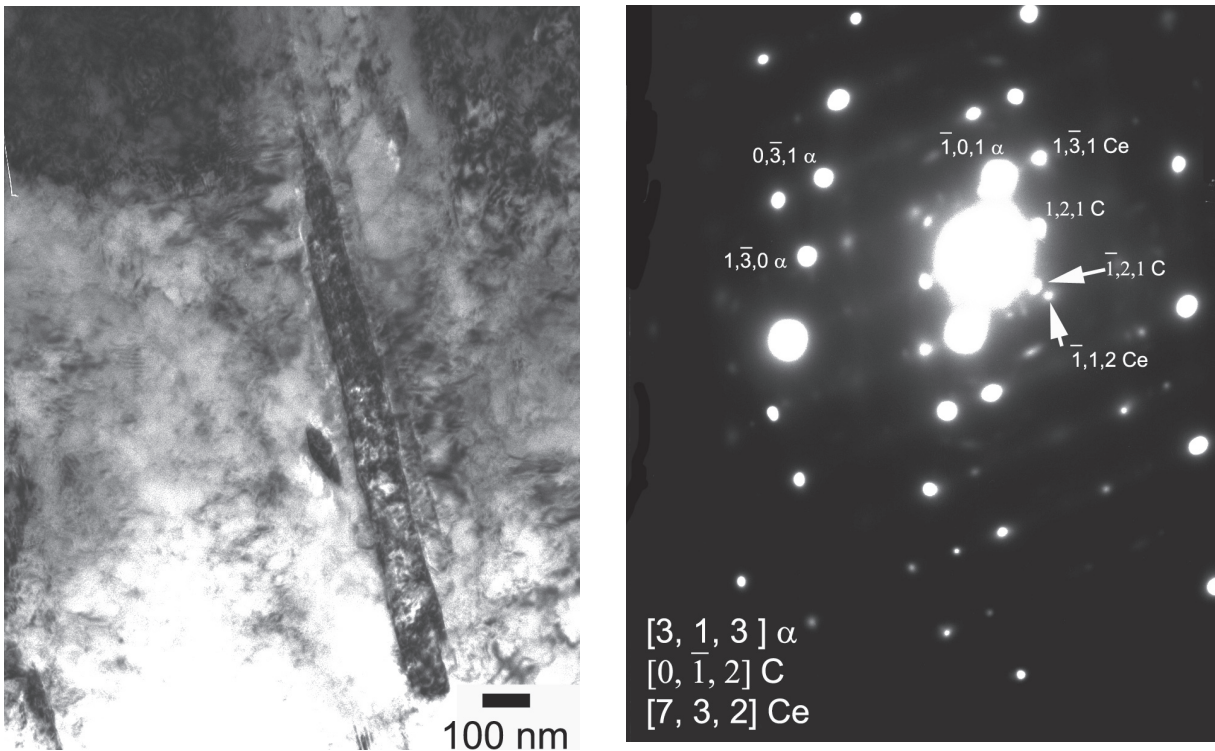


**Figure 8** Precipitates within grains and films at lath boundaries in the last bead of the 0.5 Mn weld metal illustrated using FEGSEM.
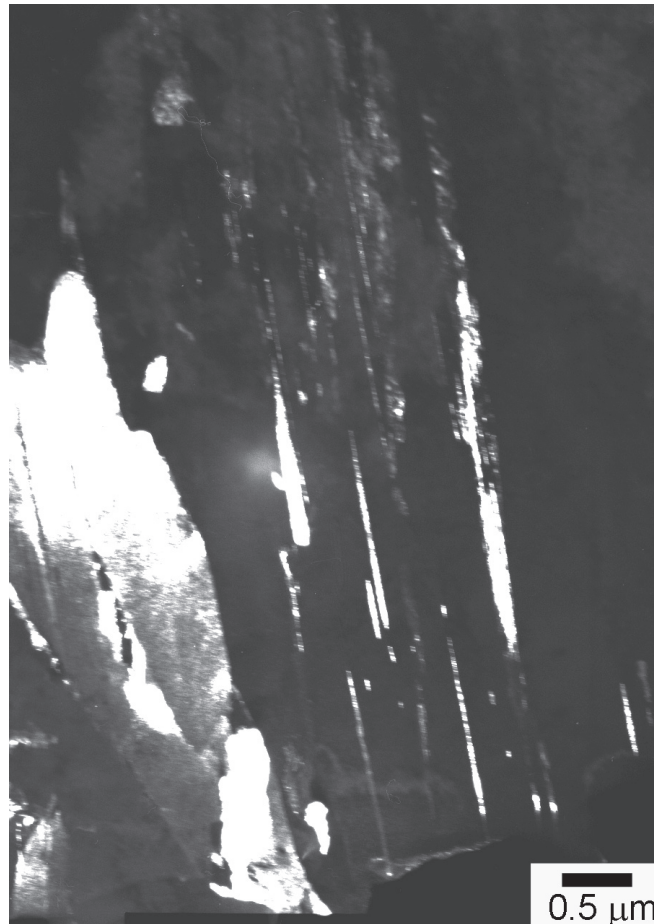
**Figure 9** FEGSEM micrograph showing martensite (M) and films at lath boundaries in the last bead of the 0.5 Mn weld metal.



**Figure 10** TEM bright field image (left) with corresponding selected area diffraction pattern (right) from the last bead of 7-2L250. The diffraction pattern shows the {3,1,3} reflections ($\alpha$) of bainitic ferrite along with the {0,−1,2} (C) and the {7,3,2} (Ce) type reflections from cementite. C and Ce represent reflections from two differently orientated families of cementite.
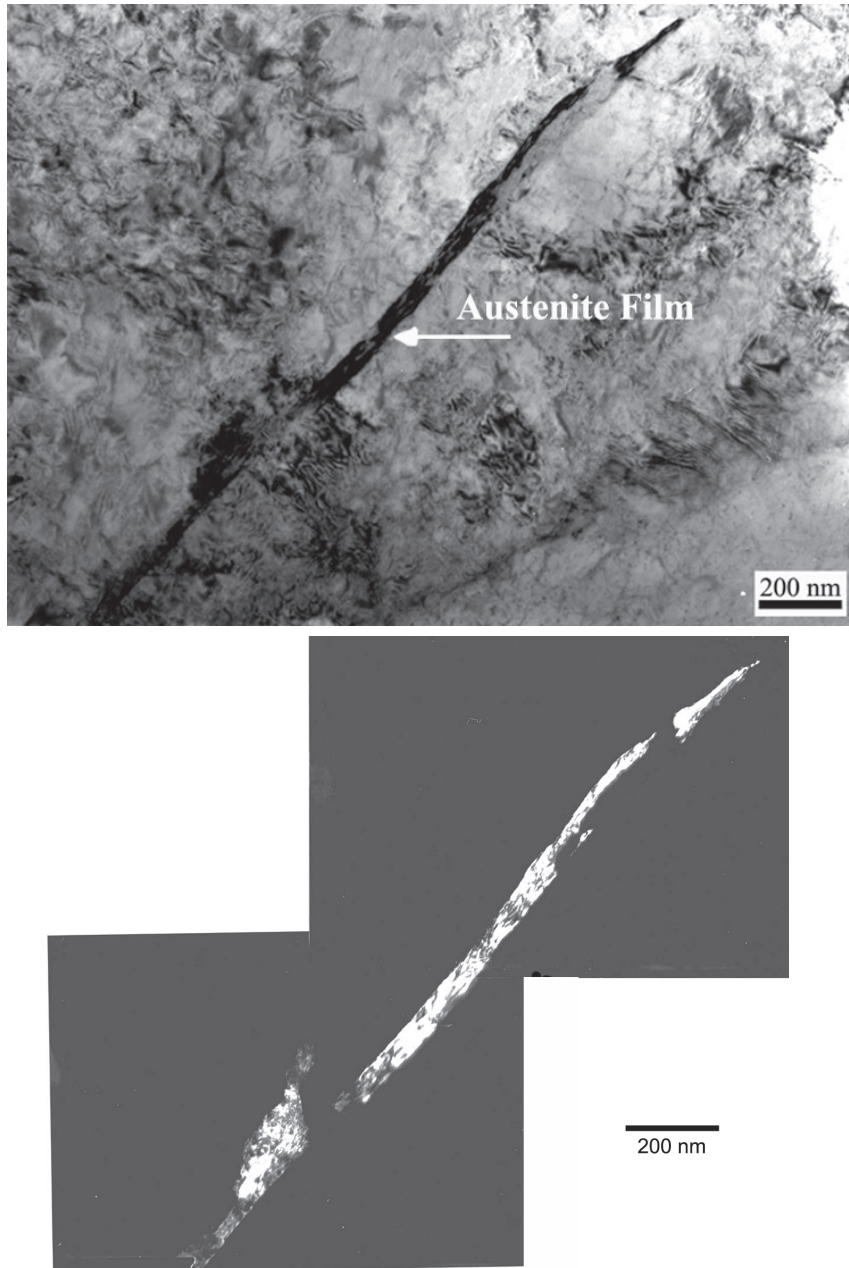
**Figure 11** TEM dark field image showing films of cementite at lath boundaries in the last bead of 7-2L250. This image was formed using the (1,2,1)C reflection in the selected area electron diffraction pattern shown in Figure 10.

mode allows the distribution of cementite to be observed as seen in Figure 11. From this work it was concluded that upper bainite was formed within the microstructure and this allows the interpretation of upper bainite in the FEGSEM micrograph shown in Figure 5. Further TEM investigations on this weld metal which characterise coalesced bainite is presented and discussed elsewhere [15]. Limited investigations with TEM on as-deposited weld metal from 7-0.5L250 were carried out. Bright and dark field images are shown in Figure 12 where a film of retained austenite was characterised using electron diffraction.

Investigations with APFIM were carried out to measure carbon in the ferritic phase. Different regions within the last bead of both the 2 and 0.5 wt. % manganese weld metals were analysed and the results of three runs from each are presented in Table 2. It is seen that the carbon level recorded in the first run with the 2 Mn weld metal was very low in comparison to the nominal level of 0.03 wt. %. The Ni and Mn levels were also slightly lower than the nominal level and it can be suggested that the sample was from a dendrite core region. The other two runs have much higher carbon levels and are compatible with the nominal level. For these runs it was found that Ni and Mn levels were higher than the nominal levels suggesting interdendritic regions. Carbon was similar to the nominal level for all runs in the 0.5 Mn weld metal. However,

10

**Figure 12** Corresponding bright and dark field images showing an austenite thin film surrounded by bainitic ferrite in the last bead of 7-0.5L250.

| Weld Metal | Ions | C | Mn | Ni | Constituent |
|---|---|---|---|---|---|
| | 34540 | 0.007 ± 0.002 | 1.89 ± 0.07 | 7.06 ± 0.29 | B |
| 7-2L250 | 4286 | 0.025 ± 0.011 | 2.27 ± 0.23 | 7.63 ± 0.78 | M |
| | 4661 | 0.055 ± 0.016 | 2.54 ± 0.23 | 7.63 ± 0.81 | M |
| | | | | | |
| | 5034 | 0.034 ± 0.012 | 0.59 ± 0.17 | 7.14 ± 0.75 | M |
| 7-0.5L250 | 72235 | 0.022 ± 0.003 | 0.46 ± 0.02 | 5.98 ± 0.18 | M |
| | 73389 | 0.027 ± 0.003 | 0.54 ± 0.03 | 6.85 ± 0.19 | M |

**Table 2** APFIM results which show the average levels of C, Mn and Ni in wt. % ± σ from individual APFIM runs along with the number of ions collected. The most likely constituent as deduced from composition is indicated where B stands for bainite and M for martensite.
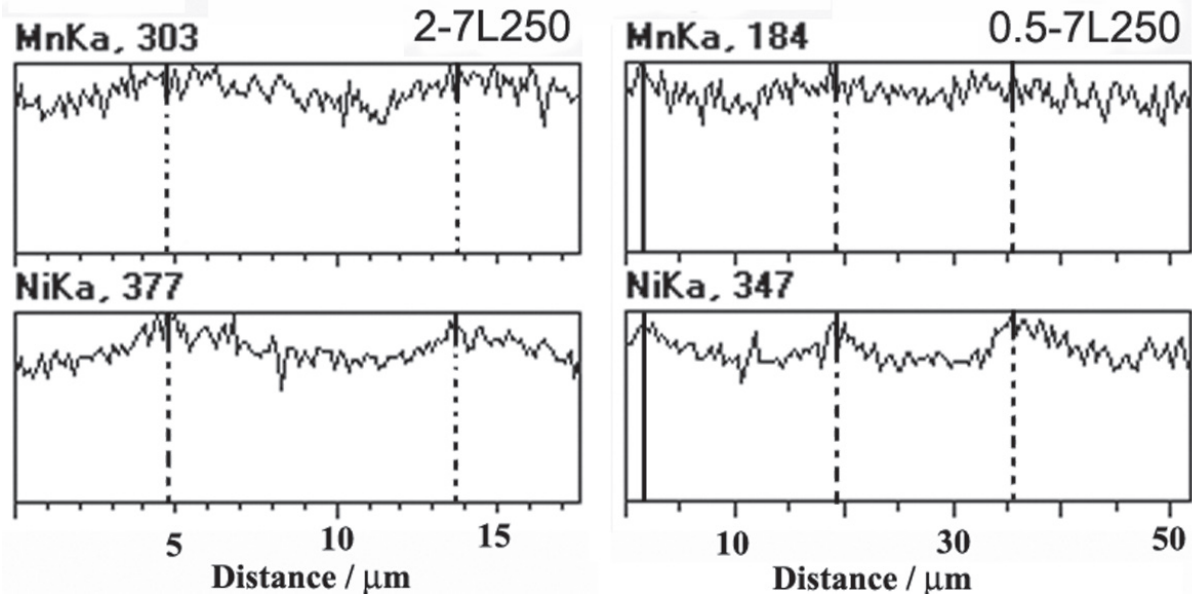
Mn was lower than the nominal levels in all runs while Ni was slightly higher with the exception of the second run where a significant depletion was seen.

**Elemental Distribution**

When the last bead was investigated with SEM in the back-scattered mode, a clear contrast was seen between the dendrite boundaries and the centres on polished samples. EDX elemental line scans were therefore carried out across the dendrites. The results are presented in Figure 13 and it is seen that the concentrations follow a wave like pattern with enrichment of Ni and Mn at the former dendrite boundary regions. EDX spot analysis was used to quantify the degree of segregation (Table 3). There is a slight overestimation of the manganese concentration but the results nevertheless allow an estimate of the degree of segregation between the dendrite boundaries and the centres. Segregation of manganese is less with the leaner alloying content of 0.5 wt. % while the relative difference in nickel segregation is almost the same in both the weld metals.
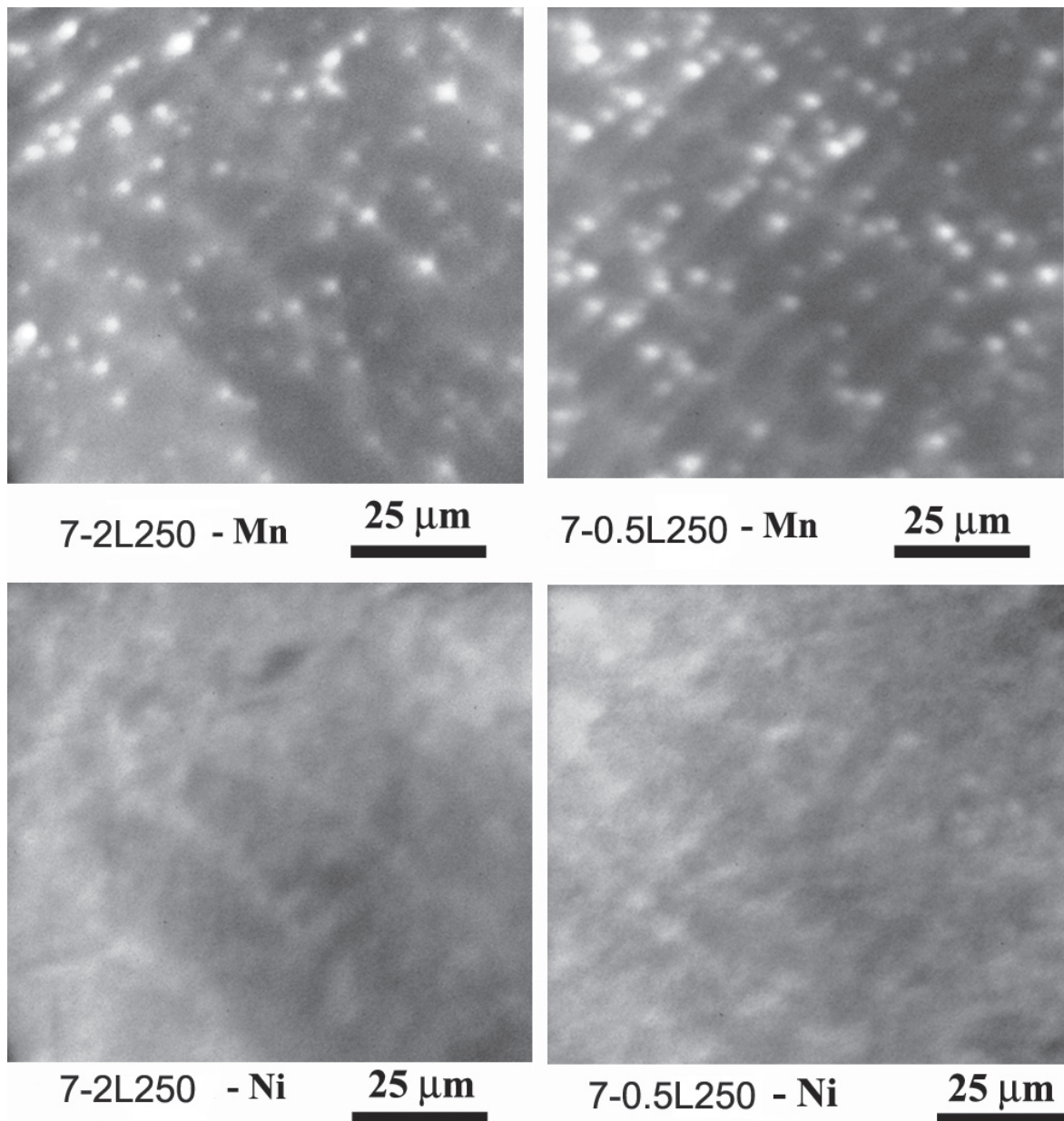
SIMS was engaged to allow the elemental segregation over a given area to be mapped; results from the last bead are presented in Figure 14. Each images shows where the individual element is concentrated by appearing brighter in contrast. It can be seen that Mn is segregated to Mn rich inclusions and to interdendritic regions while Ni was found to segregate to interdendritic regions. Overall, the results were in agreement with those obtained with EDX analysis.



**Figure 13** EDX elemental line scans across former dendrites in the last bead showing segregation of nickel and manganese. Dendrite boundary regions are indicated with broken lines.

| Weld Metal | Mn | Ni |
|---|---|---|
| 7-2L250  Boundary | 3.10 | 8.18 |
| 7-2L250  Core | 2.35 | 6.30 |
| 7-2L250 Difference | 0.75 | 1.88 |
| | | |
| 7-0.5L250 Boundary | 0.95 | 7.55 |
| 7-0.5L250 Core | 0.57 | 5.83 |
| 7-0.5L250 Difference | 0.38 | 1.72 |

**Table 3** Average compositions recorded in wt. % at dendrite boundary regions and dendrite core regions in the last bead using EDX spot analysis.
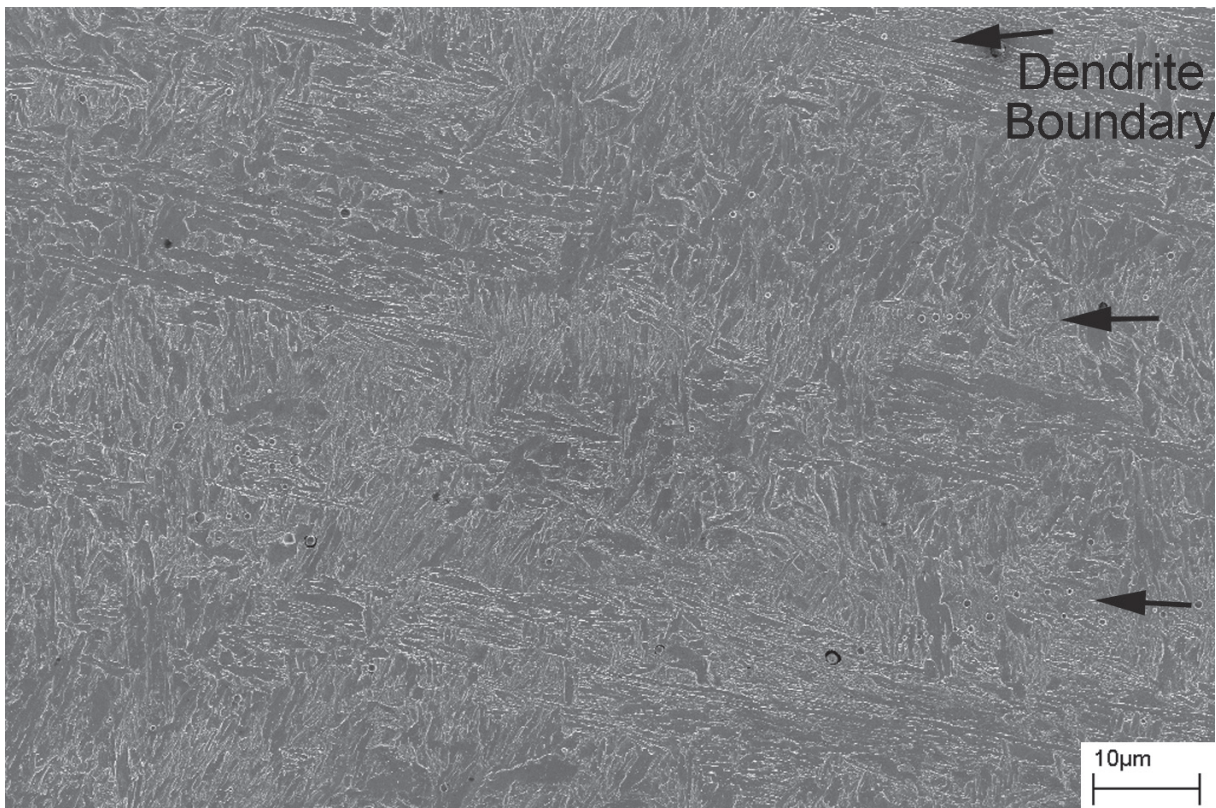


**Figure 14** SIMS micrographs showing segregation of Ni and Mn to dendrite boundaries in the last bead of 7-2L250 and 7-0.5L250.  Areas where the given element is concentrated appears brighter in contrast. Imaging of the elements was carried out using $O_2^+$ ions.

**Microstructure – reheated beads**

In regions reheated due to multiple weld passes it was still possible to distinguish the former dendrites with FEGSEM (Figure 15). It was found that the some precipitates had coarsened while other new small precipitates formed and that carbon had redistributed within the bainitic ferrite in the centre of dendrites. The plate-like precipitates were replaced by some big and numerous small spherical precipitates within the bainitic ferrite plates while more elongated precipitates were found at the plate boundaries (Figure16). A tempered martensitic microstructure was found at interdendritic regions is shown in Figure 17.
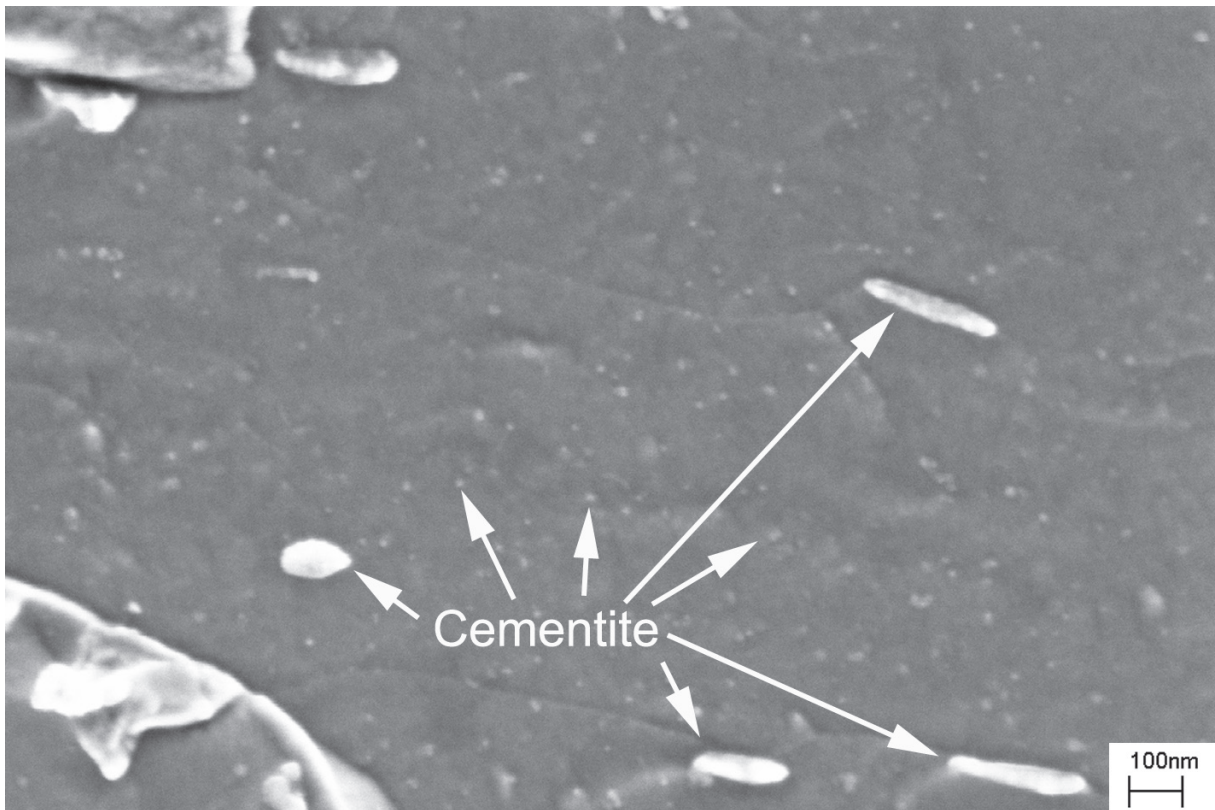
Selected micrographs are presented in Figure 18 and 19 for 7-0.5L250. Figure 18 gives an overview of the microstructure and again the dendritic structure is clearly seen. As in the high Mn weld metal it was found that carbon redistributed within bainitic ferrite in the dendrite core regions as shown in Figure 19. Spherical precipitates were found both within the grains and at the grain boundaries. At interdendritic regions a tempered martensitic microstructure was found.

Reheated regions of both weld metals were also investigated with TEM. A bright field and corresponding dark field image is shown in Figure 20 from the 2 wt. % Mn weld metal. A bainitic ferrite grain boundary region is investigated and elongated precipitates are seen at the boundary in the bright field mode. When the dark field image was formed using a cementite reflection from the selected area diffraction pattern, elongated precipitates at the boundary and small pre-
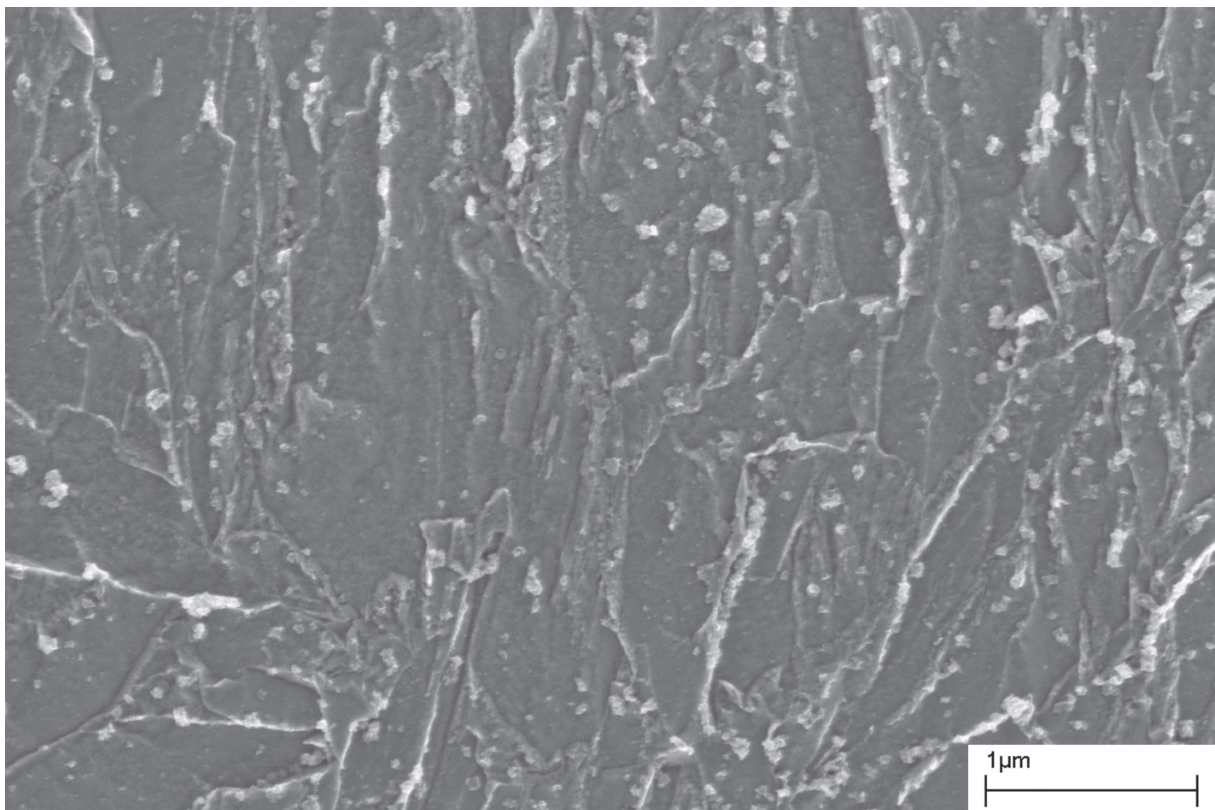


**Figure 15** The centre of a reheated bead in 7-2L250 imaged with FEGSEM clearly showing the former dendrites
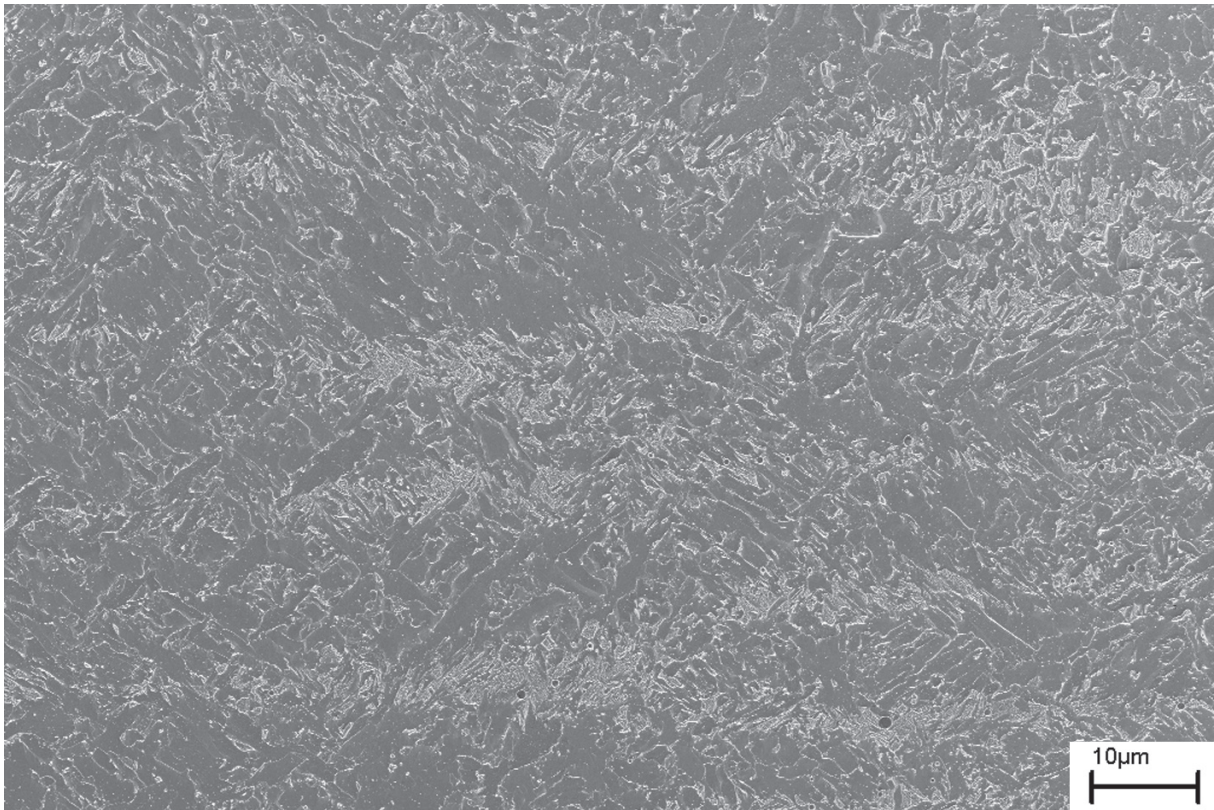
**Figure 16** High magnification FEGSEM micrograph of cementite precipitates in central regions of a former dendrite in a reheated bead of weld metal 7-2L250.
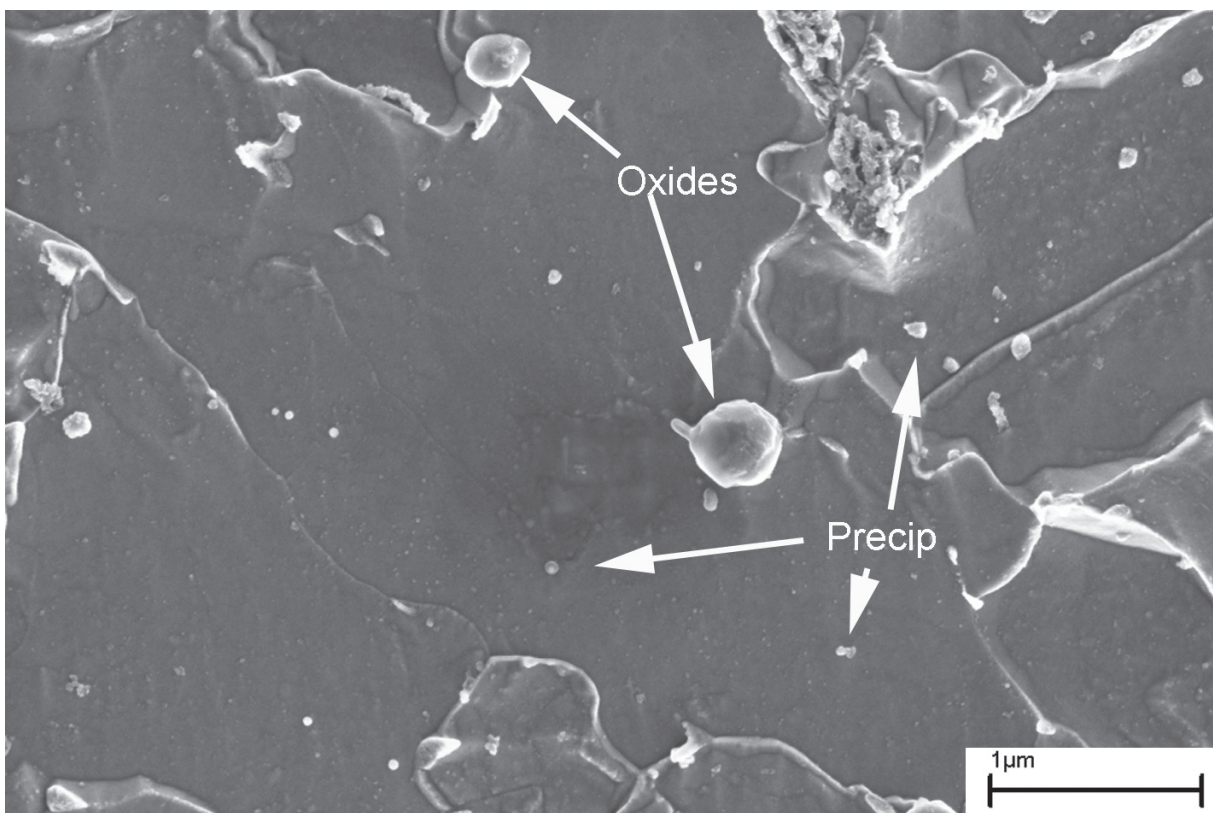


**Figure 17** A former interdendritic region in a reheated bead of 7-2L250 weld metal shown with FEGSEM. Here tempered martensite was mainly found.
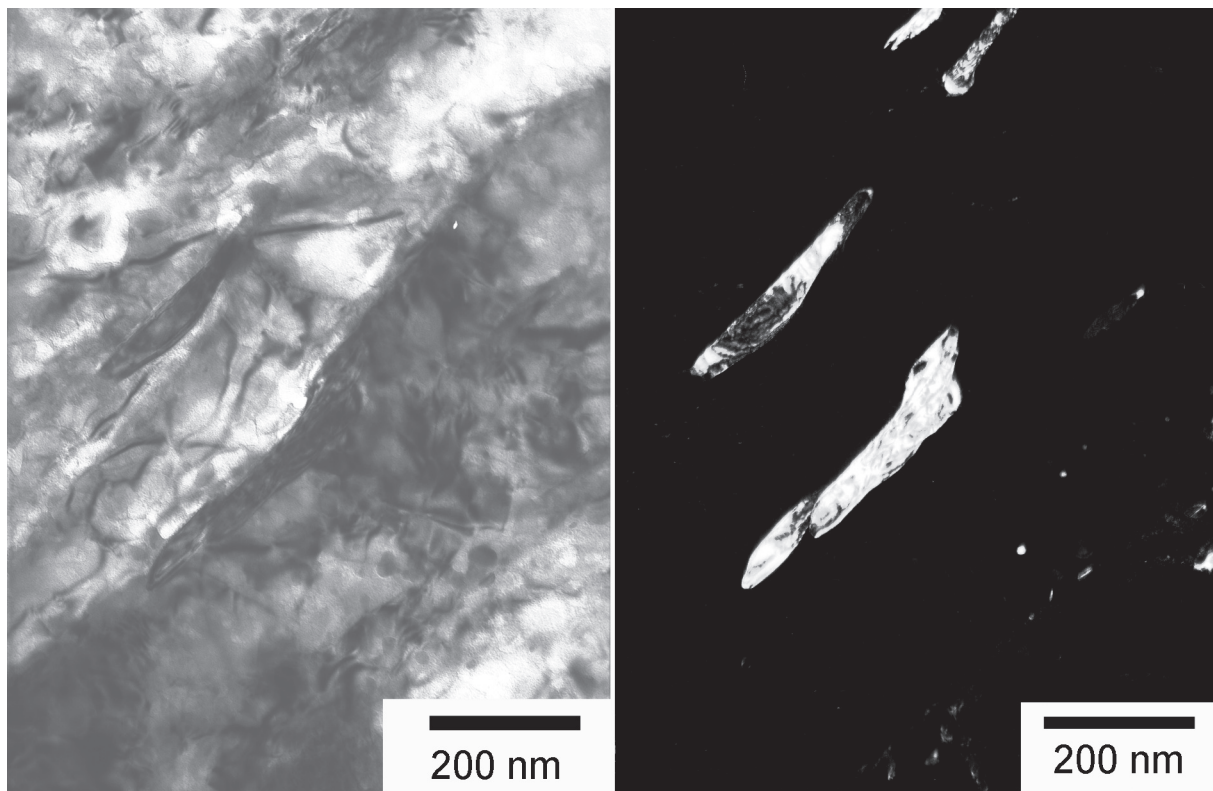
**Figure 18** Low magnification FEGSEM micrograph giving an overview on the microstructure in the centre of a reheated bead in weld metal 7-0.5L250.



**Figure 19** Precipitates in central regions of a former dendrite shown at high magnification using FEGSEM in a reheated bead of weld metal 7-0.5L250.

**Figure 20** A TEM bright field image (left) with corresponding dark field image (right) showing cementite precipitates in a reheated bead of 7-2L250 weld metal.
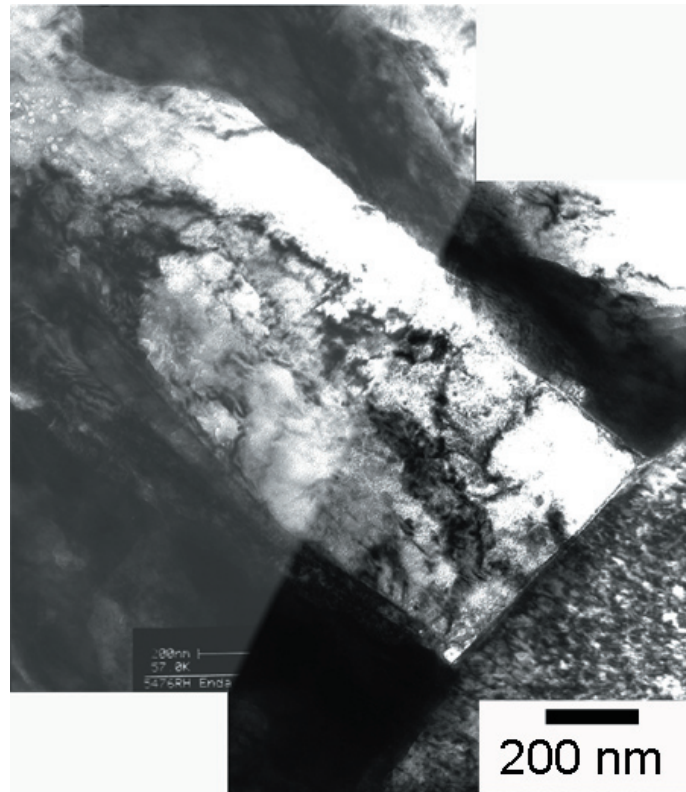
cipitates within the grains appear bright. The observed precipitates have a similar morphology to those investigated with FEGSEM in Figure 16. A bright field image of a grain in a reheated bead of the 0.5 Mn weld metal is shown in Figure 21. This grain was investigated at higher magnifications and found to contain cementite precipitates. A selected area diffraction pattern with a corresponding dark field image of cementite is shown in Figure 22. The dark field was formed using a cementite reflection. These precipitates are similar in morphology to the spherical precipitates found within the bainitic ferrite grains with FEGSEM in Figures 16 and 19.
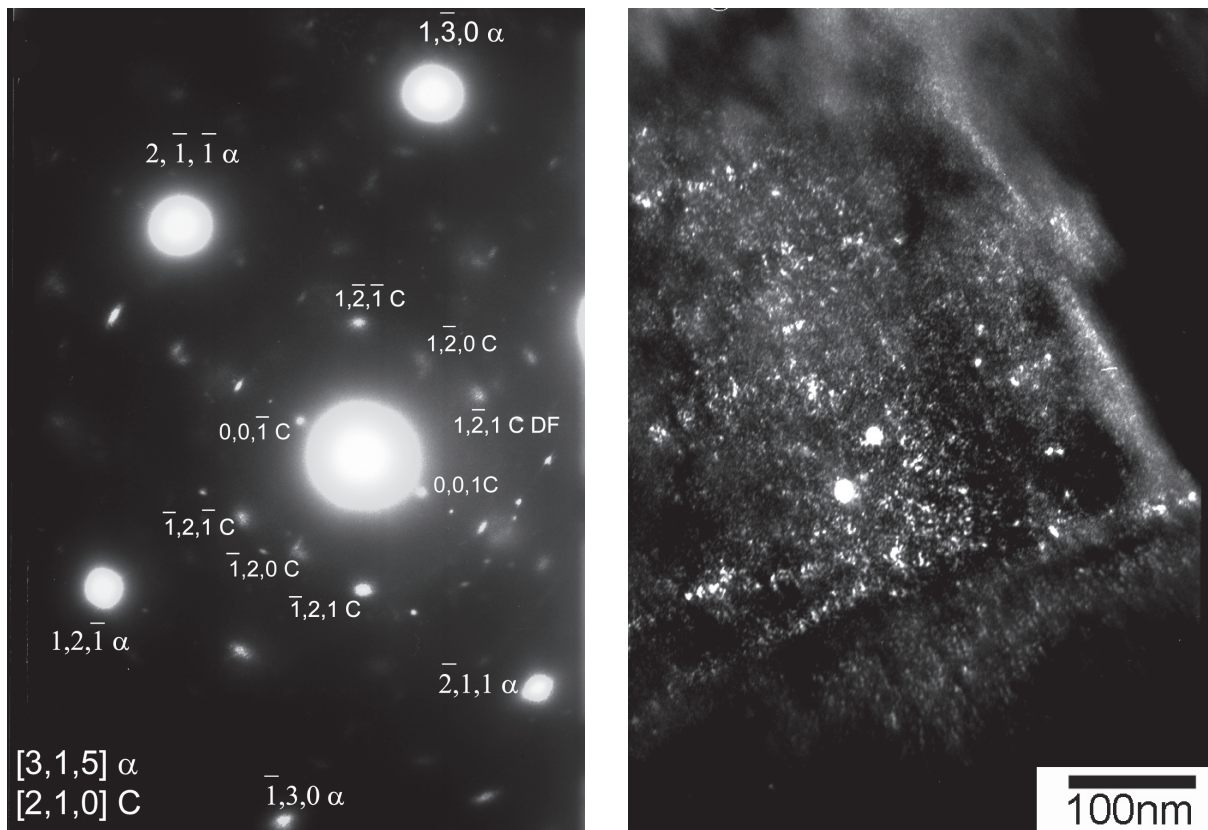
**Dilatometry**
Phase transformation temperatures were measured using dilatometry. $Ac_1$ and $Ac_3$ temperatures were measured to be 700 °C and 770 °C, respectively, for 7-0.5L250 when samples were heated at a rate of 25 °C / s. These can be compared with 690 and 740 for $Ac_1$ and $Ac_3$ for the high manganese weld metal.

On cooling it was found that austenite began to transform in the region of 490 °C when cooled at a rate of approximately 40 °C / s and at 480 °C when cooled at 1 °C / s for the 0.5 Mn weld metal. These values may be compared with 373 °C and 390 °C for the 2.0 Mn weld metal when samples were cooled at a rate of 25°C / s and 1 °C / s, respectively.

**Figure 21** A TEM bright field image of a grain in a reheated bead of 7-0.5L250 weld metal.



**Figure 22** A selected area diffraction pattern from the grain shown in Figure 21 with a corresponding dark field image showing small cementite precipitates in a reheated bead of 7-0.5L250. The dark field image was formed using the (1,–2,1) C cementite reflection.

# Discussion

Both experimental weld metals were made up of martensite and different forms of bainite along with small amounts of retained austenite (Figure 12 and reference 7). Although more or less the same constituents were found, reducing manganese from 2 to 0.5 wt % promoted noticeable differences on the weld metal microstructure and properties.

## Microstructure

In both alloys, EDX and SIMS measurements showed that manganese and nickel segregate to interdendritic regions as the weld metal solidifies. As expected, dilatometry showed that austenite was stabilised to lower transformation temperatures for richer Mn contents and a difference of about 100 °C was recorded between the 2 and 0.5 Mn levels. A similar trend was recorded when the nickel content was increased from 7 to 9 wt% at 2 wt. % Mn as is presented elsewhere [8]. This is in agreement with more of the low transformation constituents martensite and coalesced bainite forming in the the 2 Mn weld metal rather than upper bainite which forms at higher temperatures. It also explains why martensite was found mainly in former interdendritic regions where alloying content was richer.

From FEGSEM and TEM studies it was evident that mainly upper bainite formed in the 0.5 Mn weld metal (Figures 5 and 7), while significant amounts of coarse grained coalesced bainite and martensite exist with 2 Mn. Furthermore, with APFIM it proved possible to measure the local carbon content and to distinguish between martensite and bainite. These measurements reaffirmed FEGSEM and TEM results that both constituents are present with 2 Mn and also that martensite was present with 0.5 Mn. Numerous cementite platelets were formed within the bainitic ferrite grains with 2 Mn (Figure 6) while fewer precipitates were developed with 0.5 Mn (Figure 8). This is in agreement with the fact that the bainitic ferrite grains are smaller in the 0.5 Mn weld metal resulting in shorter diffusion distances to boundaries. Carbon also has a greater mobility at the higher transformation temperature measured with 0.5 Mn. Addition, thermodynamic calculations [19] show that Mn is a strong cementite stabiliser and that greater amounts of precipitates therefore are likely to develop in the 2 Mn weld metal.

## Mechanical Properties

Since mechanical properties are recorded in reheated regions it is necessary to have an understanding of the tempered microstructure. It was found that $Ac_1$ and $Ac_3$ were slightly reduced with high Mn content and it follows that more of the underlying beads are transformed back to austenite on the deposition of new weld metal. In both weld metals tempered martensite was the main microstructure at the interdendritic regions while generally tempered bainite was present at dendrite core regions. Cementite was observed in the form of elongated films at bainitic ferrite plate boundaries and as precipitates within the plates in the 0.5 Mn weld metal. In the high Mn weld metal it was found that carbon was redistributed in the bainitic ferrite with cementite coarsening and spheroidising. Numerous very small precipitates (Figure 16) were also found

and it is believed that these were newly formed from the carbon dissolved in the matrix on tempering.

The poor toughness associated with the 2 Mn weld metal was attributed to the larger grain size of the coalesced bainite. Also from dilatometry measurements it can be concluded that less tempering and more reaustenitisation takes place within the 2 Mn weld metal as a result of lower $Ac_1$ and $Ac_3$ temperatures. This contributes to greater amounts of less tempered microstructure. In the 0.5 Mn weld metal, upper bainite with a smaller grain size was dominant within the microstructure. This weld metal also experienced more tempering since Ac temperatures were higher. Further discussions of the mechanical properties are presented elsewhere [14].

## Conclusions

Two 7 wt. % nickel experimental weld metals were produced where manganese was varied at 0.5 or 2 wt. %. It was found that reducing manganese content leads to a large increase in toughness with only a moderate reduction in strength.

High resolution investigations confirmed that the microstructure was a mixture of martensite, coalesced bainite and upper bainite along with some retained austenite. Upper bainite was the dominant microstructural constituent in the 0.5 Mn weld metal while coalesced bainite and martensite were in majority in the 2 Mn weld metal. Microstructural observations were in agreement with dilatometry experiments where manganese was found to stabilise austenite on cooling.

With EDX and SIMS it was observed and quantified that manganese and nickel segregated to former interdendritic regions leaving a leaner alloying content within the core of the former dendrites. These segregation patterns give rise to greater amounts of martensite at former interdendritic regions where the greater solute content causes the austenite to transform at lower temperatures. On the contrary, bainite formed at higher temperatures within the dendrites due to the leaner alloying content.

It was concluded that the lower impact toughness in the 2 Mn weld metal was largely due to the large grain size of coalesced bainite. Good toughness in the 0.5 Mn weld metal was attributed to a finer grain size and greater amounts of tempering taking place.

## Acknowledgements

## References

1. L.-E. Svensson: Svetsaren, 54, January (1999).
2. The right welding wire could help the U.S. Navy save millions, Welding Journal, pp 55 – 58, June 1999.
3. D.J. Widgery, L. Karlsson, M. Murugananth & E. Keehan, Approaches to the devel opment of high strength weld metals, 2nd Int. Symposium on High Strength Steel, Norway (2002).
4. Zhang Z, Farrar RA, Influence of Mn and Ni on the microstructure and toughness of C–Mn–Ni weld metals, Welding Journal 76 : (5) S183–S196 May1997
5. M. Lord: Design and Modeling of Ultra – High Strength Steel Weld Deposits, Ph. D. Thesis, (1999), University of Cambridge: Cambridge.
6. Y. Kang, H.J. Kim, and S.K. Hwang: ISIJ International (Japan), 40 December (2000), p. 1237.
7. M. Murugananth, H. K. D. H. Bhadeshia, E. Keehan, H. O. Andrén, L. Karlsson, Strong and Tough Ferritic Steel Welds, Proc. 6th Int. Seminar, "Numerical Analysis of Weldability", Austria (2001)
8. E. Keehan, L. Karlsson, H.-O. Andrén, Influence of C, Mn and Ni contents on micro structure and properties of strong steel weld metals, Part I. Effect of nickel content, In Manuscript
9. SSAB Oxelösund, WeldCalc, Version 1.0.0, 98 – 99.
10. M. K. Miller, A. Cerezo, M. G. Hetherington, G. D. W. Smith, Atom Probe Field Ion Microscopy, Clarendon Press, Oxford, 1996, p. 483.
11. H. O. Andrén, H. Norden, Scand. J. Metall. 8 (1979) p.147.
12. H. O. Andrén, J. Phys. 47 (C7) (1986) p. 483.
13. U. Rolander, H. O. Andrén, J. Phys. 50 (C8) (1989) p. 529.
14. E. Keehan, M. Murugananth, L. Karlsson, H.-O. Andrén, H. K. D. H. Bhadeshia, New developments with C–Mn–Ni high strength steel weld metals, Part B. Mechanical Properties, In Manuscript
15. E. Keehan, H. K. D. H. Bhadeshia, H.-O. Andrén, L. Karlsson, L.-E. Svensson, Micro structure characterisation of a high strength steel weld metal containing the novel con stituent coalesced bainite, In manuscript
16. K.W. Andrews, D. J. Dyson, S. R. Keown, Interpretation of Electron Diffraction Pat terns, 2nd Ed., Adam Hilger Ltd., London (1971).
17. J. W. Edington, Practical Electron Microscopy in Material Science, The Macmillan Press Ltd., London (1975)
18. http://cimesg1.epfl.ch/CIOL/ems.html

19.     NPL Materials Center, National Physical Laboratory, Thermodynamic model, version 4.73 For LNX RH 7.3, 2002–11–15